JMEPEG (2012) 21:977–984
DOI: 10.1007/s11665-011-9973-5

1059-9495/$19.00

DSC Study on Phase Transitions and Their Correlation with Properties of Overaged Al-Zn-Mg-Cu Alloys

X.M. Li and M.J. Starink

(Submitted February 21, 2011; in revised form April 18, 2011)

This article investigates the phase transitions of complex quaternary Al-Zn-Mg-Cu alloys with Zr addition at overaged conditions. Differential scanning calorimetry (DSC) is employed to quantitatively analyze the phase transformation phenomena of a wide range of 7xxx series alloys through endothermic and exothermic reactions. The DSC observations detailing heat effect peaks and thermal parameters of η′ dissolution contain valuable information on the presence of equilibrium phases and the optimum alloying element contents. Based on DSC experimental data and phase diagrams, the balance of critical properties such as strength and electrical conductivity of Al-Zn-Cu-Mg 7xxx series alloys has been studied by considering the formation, dissolution, and incipient melting of S and T phase, dissolution of η′ phase as well as the formation of η phase. Nine Al-Zn-Mg-Cu alloys have been studied through microstructural examination and detailed DSC analysis. The correlation between the properties and the DSC data of the selected alloys has been analyzed.

Keywords Al-Zn-Mg-Cu alloys, correlation, differential scanning calorimetry, phase transitions, properties

1. Introduction

Al-Zn-Mg-Cu (7xxx series) alloys have attracted substantial attention of materials researchers in recent years due to the multiple demands from aerospace and transport industry for optimal properties of this series of alloys (Ref 1-5). The overall properties such as strength, toughness, and stress corrosion cracking (SCC) resistance of these alloys are largely determined by the equilibrium and metastable phases. However, detailed investigation of phase transformation with an aim to predict the properties of Al-Zn-Mg-Cu alloys with Zr addition is still lacking. Existing literature indicates that differential scanning calorimetry (DSC) can provide useful information on phase transitions through exothermic and endothermic reactions in the studies of metallic alloys (Ref 6-9). The phase transitions mainly involve the formation and dissolution of GP zones, η′, η, T, S, and Al_3Zr phase (GP zones are so-called Guinier-Preston zones, Ref 10). T is a quaternary phase based on $Mg_3Zn_3Al_2$, S is Al_2CuMg (Ref 11). The balance of properties of 7xxx alloys can be optimized by microstructural modifications via alloy compositional changes and heat treatment. Previous research (Ref 12-16) indicates that coarse intermetallic particles (larger than 1 μm) are generally detrimental to the properties, especially to the toughness. In 7xxx alloys these coarse particles are particularly the iron-rich phase (Al_7Cu_2Fe), S phase and T phase.

In view of the current progress in this area, Marlaud et al. (Ref 2) studied the influence of alloy composition and heat treatment on precipitates in three Al-Zn-Mg-Cu alloys and found that the gradual increase in the Cu of the precipitates during the aging heat treatment was essentially related to the slower diffusivity of this element in aluminum. A recent article by the Li and Starink (Ref 3) investigated the effect of alloying elements on the characteristics of intermetallic particles in two Zr-containing and two Cr-containing Al-Zn-Mg-Cu alloys at overaged conditions. Studies on optimizing the Ti and Zr content in Al-Zn-Mg-Cu-Zr alloy AA7010 containing Sc have been reported by Kumar et al. (Ref 17). Gao et al. (Ref 18) used DSC as an analytical tool for defining phases in ultrafine-grained metals processed by severe plastic deformation (e.g., 2024 and 7075 aluminum alloys) and claimed that DSC provided reproducible information for microstructural characterization. However, although it is convinced that DSC heat effects contain substantial information on phase transitions of 7xxx alloys, quantitative DSC analysis of phase transitions and the correlation between the DSC data and the properties of this series of alloys have rarely been reported.

While the SCC experiments are time consuming and the SCC resistance is difficult to quantify, the electrical conductivity of the alloys, however, can be used as a convenient measure to indicate the relative SCC resistance (Ref 8). The objective of this article is to investigate how the DSC data can be used to optimize the balance of strength and electrical conductivity of Al-Zn-Cu-Mg 7xxx alloys via microstructural control. In this study, DSC is employed to quantitatively analyze the precipitation and dissolution of meta-stable and stable phases in these alloys, because it is sensitive to reactions of these main phases. DSC scans of nine Zr-containing alloys in various overaged conditions are presented, and the influence of compositional variations and aging treatments on DSC heat evolution will be discussed in conjunction with microstructural

X.M. Li, School of Materials Science and Engineering, Southeast University, Nanjing 211189, People's Republic of China; and **M.J. Starink**, Materials Research Group, School of Engineering Sciences, University of Southampton, Southampton SO17 1BJ, UK. Contact e-mail: xmli6@seu.edu.cn.

examination of representative alloys. The correlation between the heat of η′ dissolution, aging time, yield strength, and electrical conductivity will be investigated.

2. Experimental Procedure

2.1 Materials

Nine Al-Zn-Mg-Cu-Zr plate alloys with Zr addition and different Zn, Mg, and Cu contents (broadly within in the range of 7075, 7010, and 7050 compositions) were studied. The alloys were produced at QinetiQ, Farnborough, UK, under contract through British Aluminium Plate. The range of chemical compositions of the alloys is shown in Table 1. All alloys were homogenized according to normal industrial practice.

Earlier efforts to assess the effect of composition on the balance of strength and electrical conductivity in 7xxx alloys indicated that Mg had the most significant influence on properties by strongly increasing strength and decreasing conductivity (Ref 19-22). Therefore the nine alloys were split into groups depending on their nominal Mg content for aging trials. The specimens for tensile test and conductivity measurement were extracted from the plates that were solution treated at 475 °C for 1 h and cold water quenched and aged by ramping at 20 °C/h to 172 °C and holding at 172 °C for the following times: alloys 3, 7, 8, 9 (1.9% Mg) for 1, 2, 4, 8 h; alloys 2, 4, 5 (2.3% Mg) for 2, 4, 8, 16 h; alloys 1, 6 (2.6% Mg) for 4, 8, 16, 32 h.

The conductivity and yield strength measurement were carried out at QinetiQ, Farnborough, UK. Electrical conductivity test blocks were extracted from the treat-treated plates to provide milled surfaces at the half thickness ($T/2$) position. The conductivity measurements were obtained using an AutoSigma 2000 instrument, three measurements being made for each value obtained. Care was taken to ensure that the test blocks were at laboratory temperature prior to measurement. Transverse tensile test pieces (gauge length 31 mm, diameter 5.64 mm) were extracted from the heat-treated plates at the $T/2$ position. The sketch of tensile sample is shown in Fig. 1. The yield strength refers to 0.2% proof strengths (measured in the rolling direction). The tensile tests were completed in accordance with BS EN 1002-1 (1990).

2.2 Testing Methods

Optical microscopy was used to reveal the grain structures of the alloys. Samples were cut at about half plate thickness along the three main planes, i.e., the LT, TS, and LS planes. (L = longitudinal rolling direction, T = long transverse and S = short transverse.) Specimens were mounted in Bakelite and ground successively with a final finish of 1200 grit. Subsequent polishing was performed using 6, 1, and finally ¼ μm diamond paste on cloth wheels under lubricants. For grain structure examination, samples were etched in 10 cm^3 H_3PO_4 plus 90 cm^3 distilled water heated to 50 °C for about 1 min. Image analysis software for Windows developed by Foster Findlay Associates Limited was employed for analysis of grain structure and particles in the samples. The image analysis package is linked to the optical microscope using a high-resolution digital camera for image acquisition (Ref 23).

Transmission electron microscopy (TEM) samples were prepared by cutting a material into a thin slice (~0.3 mm), subsequently punching it to a 0.3 mm diameter disc and grinding to thickness around 0.15 mm. The samples were electro-polished using a solution of 70% methanol and 30% nitric acid, maintained at a temperature of between −20 and −30 °C. The TEM facility was a JEOL JEM 2000FX transmission electron microscope. An accelerating voltage of 200 kV was used.

For DSC testing, a heat flux type Shimadzu DSC-50 was employed. For sample preparation, we cut samples from the plates which have been aged for various times at a single temperature typical for a T7 temper. For all the experiments, a pure aluminum reference (99.9%) with a mass and shape close to that of the sample was used. Baseline correction was performed employing experiments consisting of a single DSC run using pure Al samples. The heat flow was calibrated by measuring the heat of fusion of In and Zn as well as the heat capacity of pure Al. The temperature is calibrated by taking the deviation ΔT from the reference temperature, compared with the measured melting points of In and Zn. The DSC samples were machined from the 7xxx plates to discs 5 mm in diameter and 1 mm in height with average mass of about 63 mg. For heat flux type DSC testing, a reference material (pure Al) is involved and the signal derives from the difference of temperature between the sample and the reference. A baseline experiment needs to be carried out before the actual DSC experiment to calibrate the DSC cell. DSC experiments were performed at heating rate 10 °C/min. As standard procedure, each experiment contains three heating runs. In our figures, only the first run is used for calculation and analysis as shown in Figure 6 to 9, and the second and third runs are only used for correction for the difference of the heat capacity of sample and reference (for further DSC details, see Ref 6, 20, 24).

Table 1 Chemical compositions of the experimental alloys (wt.%)

Alloy no	Zn	Mg	Cu	Zr
1	5.1	2.9	1.9	0.12
2	6.1	2.3	1.9	0.12
3	6.7	1.9	1.9	0.12
4	6.1	2.3	1.2	0.12
5	6.1	2.3	2.6	0.12
6	6.7	2.9	1.9	0.12
7	5.1	1.9	1.9	0.12
8	6.7	1.9	1.2	0.12
9	6.7	1.9	2.6	0.12

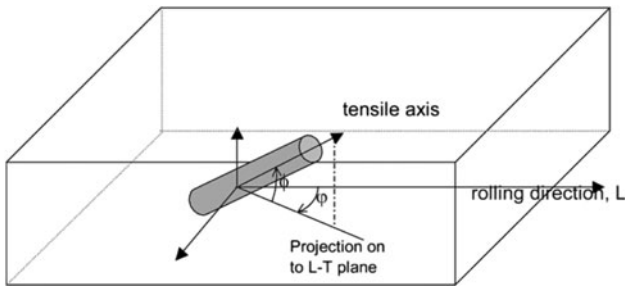

Fig. 1 Sketch of sample location in alloy sheet for tensile test

3. Results and Discussion

3.1 Microstructure

Microstructural observations were carried out for selected representative alloys. The samples were solution treated at 475 °C, quenched and then aged at 172 °C for various times (a typical T7 condition). Grain structure, intermetallic particles, precipitates as well as phase transformation evolution were studied using various techniques. Optical microscopy revealed that all alloys have largely similar grain structure: partially recrystallized with about 40% recrystallized area fraction, unrecrystallized grains display circles similar to a pan-cake shape. Coarse intermetallic particles are dispersed across the grains; these particles are mainly undissolved S phase and Fe-rich phase (Ref 3, 16, 20). Optical microstructure for alloy 2 is presented in Fig. 2, showing recrystallized areas (see Fig. 2a), and pan-cake shaped grains as well as coarse intermetallic particles (see Fig. 2b).

TEM experimental results for alloy 6 aged at 172 °C for 16 and 4 h are presented in Fig. 3. TEM investigation revealed the fine microstructure features of the alloys: precipitates in the matrix, grain (or subgrain) boundaries, and precipitate free zones (PFZ). In Fig. 3(a), bigger precipitates decorating the grain (or subgrain) boundaries correspond to the equilibrium η phase (Ref 25). The coarse η precipitates are about 50 nm in diameter. In Fig. 3(b), the size of the precipitates in the matrix is about 10-30 nm in diameter. It is observed that the precipitates for long aging time (16 h) are much coarser than the ones for short aging time (4 h), see Fig. 3(a) and (b). PFZs adjacent to the boundaries are also observed. The formation of PFZs is due to two reasons: first, there is a narrow (∼50 nm) region either side of a grain boundary which is depleted of solute due to the diffusion of solute atoms into the boundary where relatively large precipitates are formed; secondly, depletion of vacancies to levels below that needed to assist with nucleation of precipitates at the particular aging temperature.

The microstructural assessment of the alloys is important for verification of phase transitions during heat treatment, as DSC cannot directly reveal microstructural features of the tested alloys. Since quantitative TEM testing is difficult and uneconomical, it is not possible to test all the nine alloys at various aging conditions. However, using DSC technique in conjunction with microstructural examination will lead to a satisfactory investigation into the phase transformation of these alloys. It should be noted that DSC experiments are not capable of precisely detecting the minor phases in the heat effect peaks. Also, recrystallization of the grain structure will affect the kinetics of the phase transformations to some extent. Nevertheless, since the phase transitions of 7xxx series alloys involve predominately the precipitation of η, S, and T phases, which is the main focus of this study, detailed DSC analysis can still be valuable, as will be discussed below.

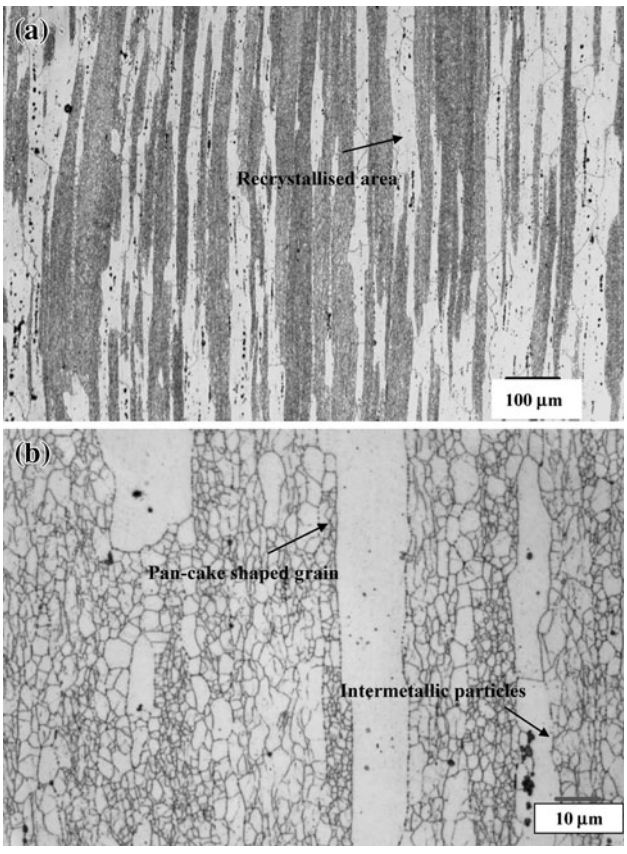

Fig. 2 Optical micrographs of Al-6.1Zn-2.3Mg-1.9Cu (wt.%) alloy (alloy 2), showing recrystallized areas (light area), pan-cake-shaped unrecrystallized grains and coarse intermetallic particles. Orientation: (a) LS, (b) TS

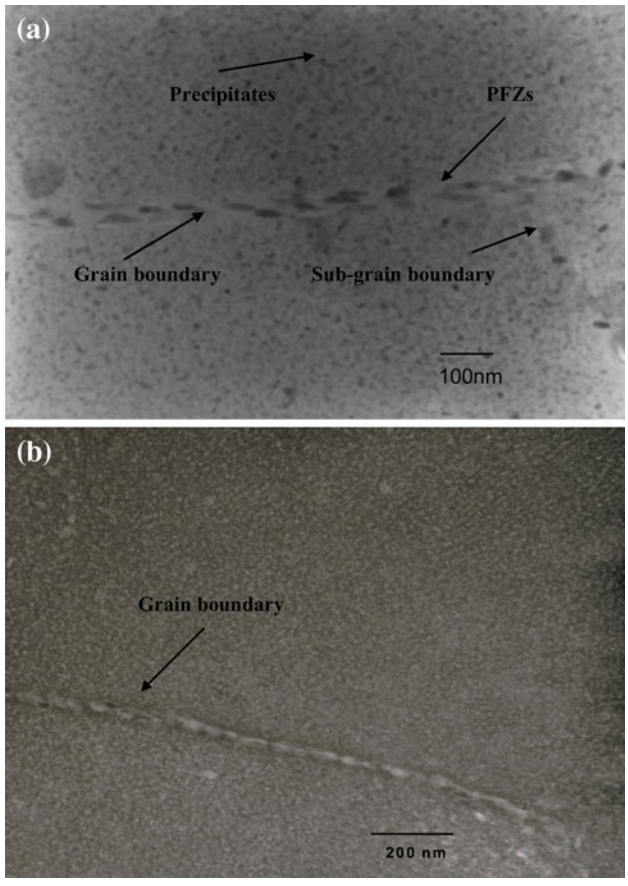

Fig. 3 TEM micrographs of the Al-6.7Zn-2.9Mg-1.9Cu (wt.%) alloy (alloy 6) aged at 172 °C. (a) 16 h, (b) 4 h, both showing precipitates, sub-grain boundary and narrow precipitate free zones adjacent to the boundaries (bright-field, B = [100])

3.2 DSC Analysis

DSC experiments were performed on samples which were solution treated and aged at 172 °C for four different aging times. All nine samples were tested.

During DSC heating and cooling the precipitation and dissolution reactions in the sample are reflected by a number of heat effects in the DSC curves. Figure 4 shows DSC curves of alloy 5 aged at 172 °C for 16 h. Comparison with other work, Ref 3, 6, 12, 26 allows identification of the heat effects: peak A corresponds to the dissolution of η′, B is the formation of η, and C the dissolution of η. Effects D and E are ascribed to the formation of S phase and the dissolution of S phase, respectively. As will be discussed below, this identification is consistent with solvus data of S phase to be presented in below. Effect G is due to the melting of undissolved S phase. Effect F corresponds to the melting of T phase and is only observed in the third DSC run. This indicates that after very slow cooling (2 °C/min), there was not sufficient time for the coarse T phase to be completely dissolved, and hence a melting of T phase occurred at 480 °C. The difference among the three DSC runs is caused by the heating cycles of DSC, for instance, in the second run the first exothermic peak corresponds to the η′ precipitation and there is a GP zone dissolution effect prior to the η′ precipitation effect.

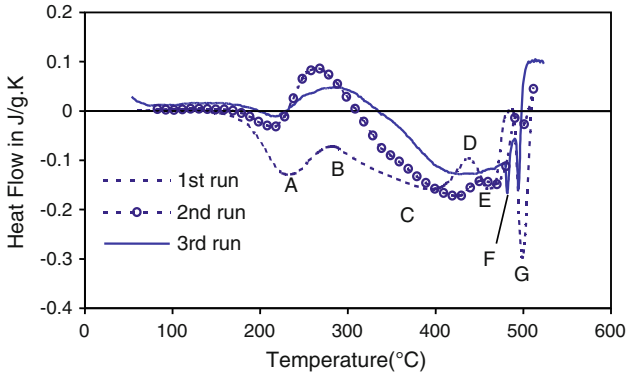

Fig. 4 DSC three runs of Al-6.1Zn-2.3Mg-2.6Cu (wt.%) alloy (alloy 5) aged at 172 °C for 16 h, showing the main heat effects: effect A corresponds to dissolution of η′, effect B precipitation of η, effect C dissolution of η, effect D formation of S phase, effect E dissolution of S, effect F melting of T phase, effect G melting of S phase. Heating rate: 10 °C/min

The nine Zr-containing Al-Zn-Mg-Cu alloys aged at 172 °C for 8 h were studied using DSC, and the main DSC effects observed, along with an attempt at identification of these effects are summarized in Table 2. The onset melting temperature of T and S phases has been measured and is tabulated in Table 3. The start melting temperature of T and S phases for the nine alloys is consistent, i.e., the melting temperature of T is about 480 °C, and the melting temperature of S is about 490 °C.

In order to further analyze the DSC data and study the correlation between the DSC data and properties, the reaction parameters were measured from DSC curves. The parameters are peak temperature of η′ dissolution T_p, end temperature of η′ dissolution T_e, heat flow at 190 °C, and heat of η′ dissolution ΔQ, as presented in Table 4. The illustrative graph for measuring the thermal parameters of η′ dissolution is given in Fig. 5. ΔQ was calculated by integrating the area from start temperature to end temperature T_e. The negative value denotes an endothermic reaction. From Table 4 it is found that, overall, $T_{p(\eta')}$, $T_{e(\eta')}$, and $\Delta Q_{(\eta')}$ vary in a consistent manner with increasing aging time, i.e., they all increase as aging time increases.

The influences of different Zn, Mg, and Cu contents on DSC curves of alloys aged at 172 °C for 8 h are shown in Fig. 6 to 9. In Fig. 6, alloy 1 has low Zn (+Cu): Mg ratio and alloy 3 has high Zn (+Cu): Mg ratio while the ratio for alloy 2 is medium. The Cu content for three alloys is constant at 1.9 wt.%. It is observed that alloy 1 with low Zn (+Cu): Mg ratio presents a very sharp endothermic peak which corresponds to the melting of S phase. The heat effects of S melting decrease with increasing the Zn (+Cu): Mg ratio. This result is consistent with the phase diagrams (see Fig. 10), which indicates that at the solution treatment temperature alloy 3 is in the α phase field, while the other two alloys are in the (α + S) phase field. A previous study (Ref 6) indicated that, to eliminate the negative

Table 2 Identification of the main effects in DSC curves of 9 Al-Zn-Mg-Cu alloys (aged at 172 °C for 8 h)

Effects	A	B	C	D	E	F	G
Alloy							
1	η′ dissolution	η formation	η dissolution	…	…	T melting	S melting
2	η′ dissolution	η formation	η dissolution	…	…	T melting	S melting
3	η′ dissolution	η formation	η dissolution	…	…	T melting	…
4	η′ dissolution	η formation	η dissolution	…	…	…	…
5	η′ dissolution	η formation	η dissolution	S formation	S dissolution	T melting	S melting
6	η′ dissolution	η formation	η dissolution	…	…	T melting	S melting
7	η′ dissolution	η formation	η dissolution	S formation	S dissolution	T melting	S melting
8	η′ dissolution	η formation	η dissolution	…	…	…	…
9	η′ dissolution	η formation	η dissolution	S formation	S dissolution	T melting	S melting

Table 3 Onset melting temperature of T and S phases (°C)

Alloy	1	2	3	4	5	6	7	8	9	Average
T phase	479.7	479.1	478.2	…	479.2	479.4	479.8	…	481.3	479.5
S phase	492.7	492.2	…	…	491.1	491.3	492.7	…	492.1	492.0

Table 4 Heat of reactions obtained from DSC curves for nine alloys for various aging times at aging temperature 172 °C

Alloy	Aging time, h	$T_{e(\eta')}$, °C	$T_{p(\eta')}$, °C	$\Delta Q_{(\eta')}$, J/g	HF at 190 °C, J/g · K
1	4	277	221	−4.51	−0.0367
	8	284	223	−5.54	−0.0433
	16	292	237	−7.95	−0.0308
	32	292	235	−8.19	−0.0303
2	2	240	214	−5.84	−0.0675
	4	275	218	−5.96	−0.0569
	8	280	224	−7.26	−0.0513
	16	288	240	−9.35	−0.0314
3	1	242	213	−4.11	−0.0547
	2	253	216	−6.36	−0.0719
	4	274	223	−7.44	−0.0448
	8	277	231	−9.20	−0.0499
4	2	226	203	−5.16	−0.1070
	4	273	213	−6.12	−0.0824
	8	276	226	−7.75	−0.0457
	16	279	230	−8.10	−0.0416
5	2	243	216	−4.04	−0.0515
	4	277	223	−5.72	−0.0426
	8	281	229	−8.04	−0.0442
	16	287	239	−9.90	−0.0371
6	4	235	215	−4.44	−0.0617
	8	268	226	−5.45	−0.0492
	16	282	228	−7.11	−0.0400
	32	284	237	−8.72	−0.0390
7	1	233	218	−5.21	−0.0581
	2	263	220	−5.50	−0.0412
	4	263	223	−7.75	−0.0555
	8	284	229	−7.89	−0.0434
8	1	251	212	−6.61	−0.0771
	2	275	217	−6.64	−0.0580
	4	278	221	−7.93	−0.0581
	8	275	228	−8.74	−0.0547
9	1	234	209	−4.34	−0.0780
	2	256	211	−4.37	−0.0576
	4	244	216	−5.83	−0.0678
	8	275	232	−8.02	−0.0391

T_p, peak temperature; ΔQ, heat of dissolution; HF, heat flow. The negative value denotes an endothermic reaction

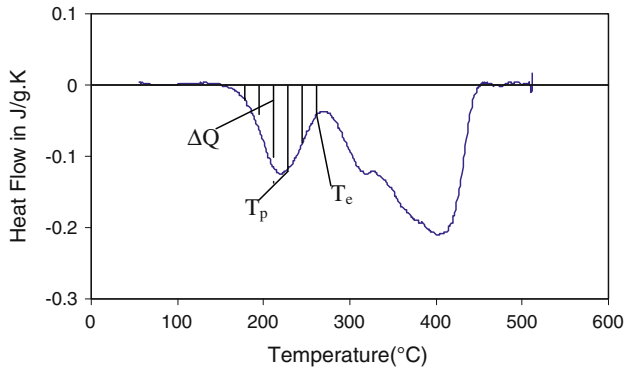

Fig. 5 Illustrative graph for measuring parameters of the η′ dissolution effect

effects of S and T phases on the properties, Zn:Mg ratio should be around 3 and the content of Zn + Mg within 12 wt.%. However, the optimum results can only be obtained when Cu

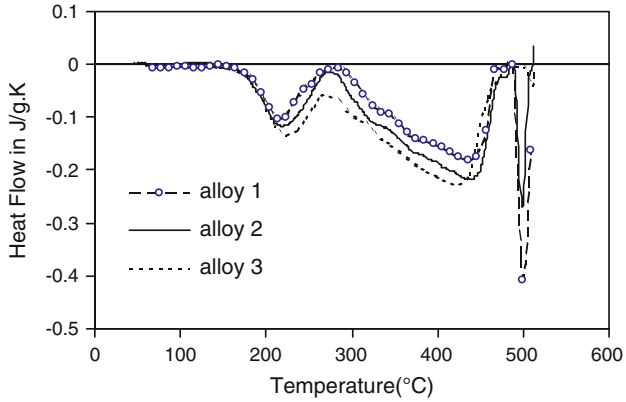

Fig. 6 DSC curves of alloys 1, 2, and 3 aged at 172 °C for 8 h. Alloy 1: low Zn (+Cu):Mg ratio; alloy 2: medium Zn (+Cu):Mg ratio; alloy 3: high Zn (+Cu):Mg ratio

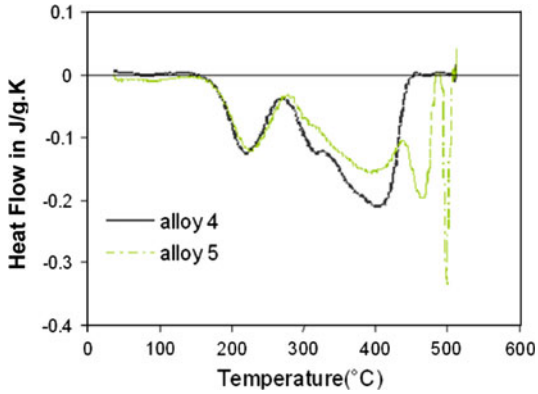

Fig. 7 DSC curves of alloy 4 and 5 aged at 172 °C for 8 h. Medium Zn:Mg and medium Mg. Alloy 4: low Cu, alloy 5: high Cu

content is about 1.9 wt.%, which is the medium among nine alloys.

In order to investigate the effect of Cu content on the S phase dissolution and melting after solution treatment, DSC curves of alloys 4 and 5 are plotted as shown in Fig. 7. As presented in Table 1, alloys 4 and 5 have medium Zn:Mg ratio and medium Mg, the Cu content of alloy 4 (1.2 wt.%) is low and that of alloy 5 (2.6 wt.%) is high. From Fig. 6 it is observed that for alloy 5 the high Cu content results in a strong peak for S melting due to the presence of S phase (Ref 12, 19), while for alloy 4 with low Cu content, no S phase is observed. These observations on S phase content are consistent with the solvus data for S phase plotted in the phase diagram in Fig. 10. These solvi were calculated using a regular solution model as outlined in Ref 20. In this model, the solvus related to an intermetallic phase $M_mA_aB_bC_c$ (M is the main constituent of the alloy, and A, B, C are the alloying elements) is given by:

$$(c_A)^a(c_B)^b(c_C)^c = c_0 \exp\left[\frac{-\Delta H_{sol}}{k_B T}\right] \quad \text{(Eq 1)}$$

where ΔH_{sol} is the enthalpy of formation per $M_mA_aB_bC_c$ unit, k_B is Boltzmann's constant, and c_o is a constant. Appropriate values for ΔH_{sol}, c_o, a, b, c are derived from available solubility data (see Ref 20).

The overall effect of Zn and Mg content on phase transitions of the alloys was studied by plotting the DSC curves of alloys 6

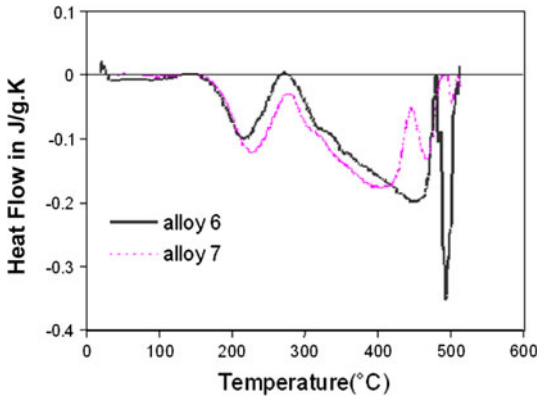

Fig. 8 DSC curves of alloys 6 and 7 aged at 172 °C for 8 h. Alloy 6: high Zn + Mg; alloy 7: low Zn + Mg

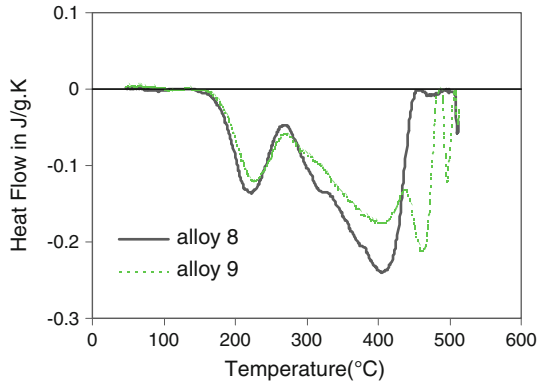

Fig. 9 DSC curves of alloys 8 and 9 aged at 172 °C for 8 h. Alloy 8: high Zn:Mg, lower Cu; alloy 9: high Zn:Mg, higher Cu

and 7. In Fig. 8, alloy 6 has high Zn + Mg content and high Mg content (2.9 wt.%), alloy 7 has low Zn + Mg content and low Mg content (1.9 wt.%), whereas Cu content remains the same for the two alloys (1.9 wt.%). The melting peak in alloy 6 starts at 480 °C, and hence, the sharp endothermic peak is ascribed to T phase and S phase melting.

For alloys with high Zn:Mg ratio, the DSC curves are shown in Fig. 9. It is clear that the sharp peak at 490 °C for alloy 9 corresponds to the S melting because of the high Cu content (2.6 wt.%) of the alloy, while for alloy 8 with low Cu content (1.2 wt.%), the S phase is not observed at all. Again these observations are consistent with the S solvus in the phase diagram (Fig. 10). Overall, the compositional variations of Zn, Mg, and Cu alloying elements have significant effects on the formation, dissolution, and melting of η, S, and T phases. These phases, when stable in equilibrium state, play a key role in determining the properties of the alloys, thus the optimized contents of the major alloying elements should be considered in the context of alloy design. However, since this study only focuses on the phase transformation behavior of the alloys as well as the effects of alloying elements, we will not discuss alloy design detailedly in this study.

3.3 Correlation Between DSC Data and Properties

A comparison of DSC data with available strength and conductivity data exhibit some interesting points. First, there is

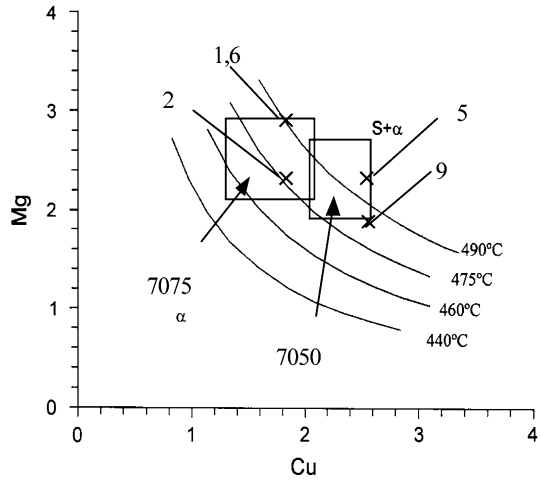

Fig. 10 Solvi of S phase in Al-Zn-Mg-Cu with Zn = 6 wt.%, temperature range 440-490 °C, showing positions of alloys 1, 2, 5, 6, and 9 in the diagram, the rest of alloys are in the compositional windows of alloy 7050 and 7075

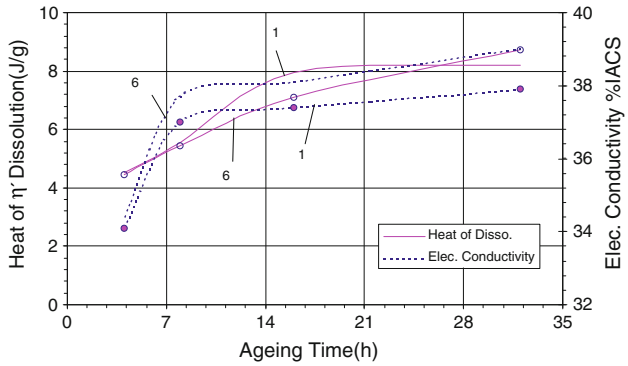

Fig. 11 Correlation between heat of η′ dissolution, conductivity, and aging time. Alloy 1: low Zn; alloy 6: high Zn, both with high Mg and medium Cu

a general trend that the heat of η′ dissolution and conductivity increase significantly with increasing aging time for all of the alloys studied, while the yield strength generally decreases with aging time. To illustrate this, the heat of η′ dissolution $\Delta Q_{(\eta')}$ and electrical conductivity during aging for alloys 1 and 6 are plotted in Fig. 11. Increase of conductivity with aging time was also evidenced for alloy 7475 (Ref 27), which has similar compositions as our experimental alloys, and these results are consistent in terms of electrical conductivity variations with aging time. Secondly, from the available data about the electrical conductivity of the nine alloys, it is observed that the conductivity increases with the increase of $\Delta Q_{(\eta')}$ value. This is because the $\Delta Q_{(\eta')}$ reflects the amount of η′ precipitates. The larger $\Delta Q_{(\eta')}$ value implies that the sample contains more η′, thus more Mg and Zn has precipitated and is "tied-up" in the η′ phase. Since alloying elements dissolved in the Al-rich phase strongly reduce its electrical conductivity (Ref 28), it is expected that the conductivity will increase as a result of the reduction of concentration of Mg and Zn in the matrix, which accompanies η′ precipitation. Thirdly, the plot of yield strength against heat of η′ dissolution $\Delta Q_{(\eta')}$, as shown in Fig. 12(a), indicates that there is a correlation between the yield strength

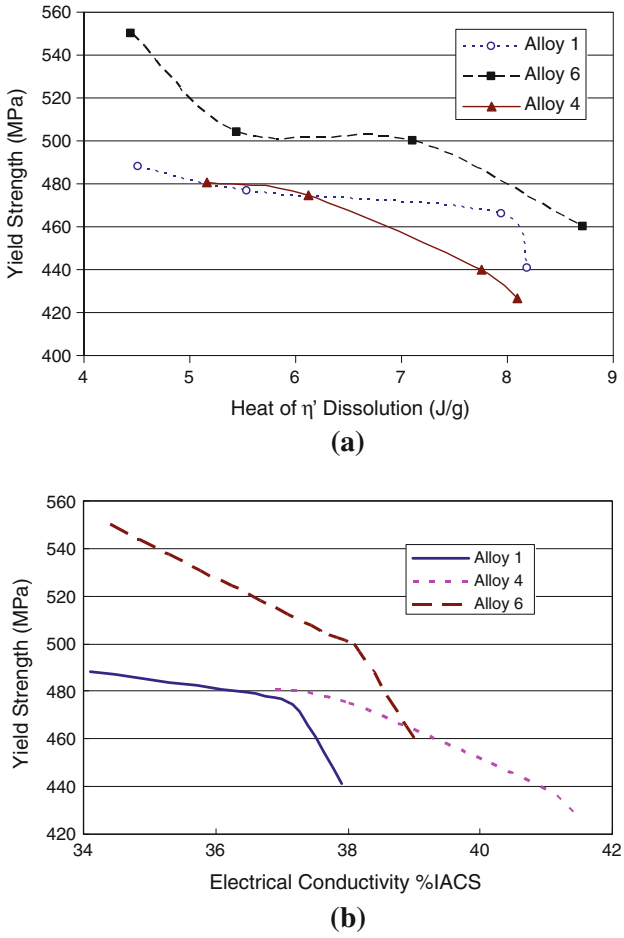

Fig. 12 (a) Correlation between heat of η′ dissolution and yield strength; (b) electrical conductivity correlated with yield strength. Alloy 1 with low Zn and alloy 6 high Zn, both with high Mg and medium Cu; alloy 4: low Cu, medium Zn and Mg

and the DSC data and the yield strength of the alloys generally increases with the increase of the heat of η′ dissolution $\Delta Q_{(\eta')}$. The data of yield strength and $\Delta Q_{(\eta')}$ for the rest of the nine alloys also display similar correlation. Correlation between electrical conductivity and yield strength is plotted in Fig. 12(b). It is shown that generally the yield strength decreases with the increase of electrical conductivity. This implies that the property of SCC resistance can be improved with the trade-off of the strength, which is in agreement with previous findings (Ref 8). There are many factors influencing the mechanical property of the alloy, and for 7xxx alloys, the strength is gained mainly through age hardening and the main precipitates η′ and η play a key role, which implies the correlation between precipitation heat effect and yield strength exist.

From above discussion, we can see that DSC is a very useful tool to analyze the phase transition and microstructural evolution of aluminum alloys, if it is combined with microscopic techniques for verification. However, some limitations and drawbacks of DSC experiments should also be addressed. For instance, sample preparation and baseline correction could influence the testing results to some extend (Ref 9, 18, 24). Nevertheless, as DSC experiments are quite economical and reproducible, there is a great potential for DSC data to be used to correlate with alloy chemistry and predict the properties of 7xxx alloys.

4. Conclusions

Quantitative analysis of the precipitation and dissolution of meta-stable and stable phases in Al-Zn-Mg-Cu alloys have been carried out in this study, because the properties of the alloys are largely determined by these main phases. DSC scans of nine Zr-containing alloys in various overaged conditions were performed and the influence of compositional variations and aging treatments on DSC heat evolution was discussed. Microstructural examination of representative alloys was also performed in support of the DSC experimental findings. The conclusions can be drawn as follows:

(1) Based on the DSC observations and phase diagrams, it was found that for the alloys with 1.9% Cu and Mg in excess of 2.1%, S phase is present. If Cu content is in excess of 1.9%, the alloys with Mg between 1.9 and 2.9% also contain S phase. For solution-treated samples, incipient melting of S phase at 490 °C was observed in DSC scans for high Cu and high Mg alloys after all aging treatments. Incipient melting of T phase at 480 °C was observed only for the alloy with high Mg and Zn contents.

(2) The detailed analysis of DSC data indicates that compositional variations of Zn, Mg, and Cu alloying elements have significant effects on the formation, dissolution, and melting of η, S, and T phases. Since these phases play a key role in determining the properties of the alloys, a better understanding of the phase transformation behavior results in the optimization of the composition in the context of alloy design.

(3) There exists a correlation between the heat of η′ dissolution, aging time, yield strength, and conductivity. Generally, conductivity increases with aging time whereas yield strength decreases with aging time. Also, with the increase of the heat of η′ dissolution, the conductivity increases and the yield strength decreases.

Acknowledgments

The financial support from Southampton University, UK and British Aluminium Plate, Birmingham, UK is gratefully acknowledged. The experimental alloys were produced and the tests of yield strength and electrical conductivity of the alloys were performed at QinetiQ, Farnborough, UK. Their technical support for this work is gratefully acknowledged.

References

1. P. Sepehrband and S. Esmaeili, Application of Recently Developed Approaches to Microstructural Characterization and Yield Strength Modeling of Aluminum Alloy AA7030, *Mater. Sci. Eng. A*, 2008, **487**(1–2), p 309–315
2. T. Marlaud, A. Deschamps, F. Bley, W. Lefebvre, and B. Baroux, Evolution of Precipitate Microstructures During the Retrogression and Re-Ageing Heat Treatment of an Al-Zn-Mg-Cu Alloy, *Acta Mater.*, 2010, **58**(14), p 248–260
3. X.M. Li and M.J. Starink, Identification and Analysis of Intermetallic Phases in Overaged Zr-Containing and Cr-Containing Al-Zn-Mg-Cu Alloys, *J. Alloys Compd.*, 2011, **509**(2), p 471–476
4. M.A. Suarez, O. Alvarez, M.A. Alvarez, R.A. Rodriguez, S. Valdez, and J.A. Juarez, Characterization of Microstructures Obtained in

Wedge Shaped Al-Zn-Mg Ingots, *J. Alloys Compd.*, 2010, **492**(1–2), p 373–377
5. F. Wang, B. Xiong, Y. Zhang, H. Liu, Z. Li, and Q. Liu, Microstructure and Mechanical Properties of Spray-Deposited Al-Zn-Mg-Cu Alloy Processed Through Hot Rolling and Heat Treatment, *Mater. Sci. Eng. A*, 2009, **518**, p 144–149
6. X. Li and M.J. Starink, Analysis of Precipitation and Dissolution in Overaged 7xxx Aluminium Alloys Using DSC, *Mater. Sci. Forum*, 2000, **331–337**, p 1071–1076
7. J.K. Park and A.J. Ardell, Precipitate. Microstructure of Peak-Aged 7075 Al, *Scripta Metall.*, 1988, **22**, p 1115–1119
8. M.J. Starink and X.M. Li, A model for the Electrical Conductivity of Peak Aged and Overaged Al-Zn-Mg-Cu Alloys, *Metall. Mater. Trans. A*, 2003, **34A**, p 899–911
9. M.J. Starink, The Analysis of Al-Based Alloys by Calorimetry: Quantitative Analysis of Reactions and Reaction Kinetics, *Int. Mater. Rev.*, 2004, **49**, p 191–226
10. J.A. Wert, Identification of Precipitates in 7075 Al After High-Temperature Aging, *Scripta Metall.*, 1981, **15**, p 445–447
11. S.K. Maloney, K. Hono, I.J. Polmear, and S.P. Ringer, The Chemistry of Precipitates in an Aged Al-2.1Zn-1.7Mg at.% Alloy, *Scripta Mater.*, 1999, **41**, p 1031–1038
12. A.J. Morris, R.F. Robey, P.D. Couch, and E.D.L. Rios, A Comparison of the Damage Tolerance of 7010 T7451 and 7050 T7451, *Mater. Sci. Forum*, 1997, **242**, p 181–186
13. M. Sharma, Microstructural and Mechanical Characterization of Various Modified 7XXX Series Spray Formed Alloys, *Mater. Charact.*, 2008, **59**(1), p 91–99
14. N. Yazdian, F. Karimzadeh, and M. Tavoosi, Microstructural Evolution of Nanostructure 7075 Aluminum Alloy During Isothermal Annealing, *J. Alloys Compd.*, 2010, **493**(1–2), p 137–141
15. M.J. Starink and S.C. Wang, The Thermodynamics of and Strengthening Due to Co-Clusters: General Theory and Application to the Case of Al-Cu-Mg Alloys, *Acta Mater.*, 2009, **57**, p 2376–2389
16. R.C. Dorward, Precipitate Coarsening During Overaging of Al-Zn-Mg-Cu Alloy, *Mater. Sci. Technol.*, 1999, **15**, p 1133–1138
17. A. Kumar, A.K. Mukhopadhyay, and K.S. Prasad, Superplastic Behaviour of Al-Zn-Mg-Cu-Zr Alloy AA7010 Containing Sc, *Mater. Sci. Eng. A*, 2010, **527**, p 854–857
18. N. Gao, M.J. Starink, and T.G. Langdon, Using Differential Scanning Calorimetry as an Analytical Tool for Ultrafine-Grained Metals Processed by Severe Plastic Deformation, *Mater. Sci. Technol.*, 2009, **23**(6), p 687–698
19. J.A. Wagner and R.N. Shenoy, The Effect of Copper, Chromium, and Zirconium on the Microstructure and Mechanical Properties of Al-Zn-Mg-Cu Alloys, *Metall. Trans. A*, 1991, **22A**, p 2809–2818
20. X.M. Li and J. Starink, The Effect of Compositional Variations on Characteristics of Coarse Intermetallic Particles in Overaged 7000 Aluminium Alloys, *Mater. Sci. Technol.*, 2001, **17**, p 1324–1328
21. T.J. Warner, R.A. Shahani, P. Lassince, and G.M. Raynaud, Aluminium Alloy Developments for Affordable Airframe Structures, *3rd ASM Conf. On Synthesis, Processing and Modelling of Advanced Materials*, Paris, France, 1997, p 77–88
22. I.J. Polmear, *Light Alloys-Metallurgy of the Light Metals*, St. Edmundsbury Press Ltd, Suffolk, UK, 1996
23. J. Boselli, P.D. Pitcher, P.J. Gregson, and I. Sinclair, Quantitative Assessment of Particle Distribution Effects on Short Crack Growth in SiCp Reinforced Al-Alloys, *Scripta Mater.*, 1998, **38**, p 839–844
24. M.J. Starink and P.J. Gregson, S′ and δ′ Phase Precipitation in SiCp Reinforced A1-1.2wt.%Cu-1wt.% Mg-x Li Alloys, *Mater. Sci. Eng. A*, 1996, **211**, p 54–65
25. T.S. Srivatsan, S. Sriram, D. Veeraraghavan, and V.K. Vasudevan, Microstructure, Tensile Deformation and Fracture Behaviour of Aluminium Alloy 7055, *J. Mater. Sci.*, 1997, **32**, p 2883–2894
26. A. Deschamps, Y. Brechet, P. Guyot, and F. Livet, On the Influence of Dislocations on Precipitation in an Al-Zn-Mg Alloy, *Z. Metallkd.*, 1997, **88**, p 601–606
27. W. Hepples, PhD thesis, University of Newcastle Upon Tyne, UK, 1987
28. J.E. Hatch, *Aluminium: Properties and Physical Metallurgy*, American Society for Metals, Metals Park, OH, 1983